A Numerical Study on the Maneuverability of the DTMB 5415 using CFD

By

Jinhae Kim

Submitted for the Degree of Master of Philosophy

Department of Naval Architecture, Ocean and Marine Engineering

University of Strathclyde

June 2018

Declaration of Authenticity and Author's Rights

This thesis is the result of the author's original research. It has been composed by the author and has not been previously submitted for examination which has led to the award of a degree.

Signed:

Date:

Acknowledgements

I would like to thank my supervisor Dr. Tahsin Tezdogan of the Department of Naval Architecture and Marine Engineering at the University of Strathclyde. He has reviewed this paper and provided me appropriate feedback with the proper study environment. I also would like to thank for my Korean supervisor Prof. Sang-Hyun Kim of the Department of Naval Architecture and Ocean Engineering at Inha University, South Korea. He suggested me to get an opportunity for studying at the University of Strathclyde.

I would like to appreciate to my college and friend. Even if I did not discuss this study, this article may not be completed. They inspired me whenever I study with them. And they were eager to their own research. It stimulates my passion for study.

I would also like to thank professors who made Korea-UK Global Engineer Education Programme for Offshore Plant and all people who take charge of this project. Thanks for their effort, I was able to study at University of Strathclyde.

Jinhae Kim

Abstract

The International Maritime Organization (IMO) has proposed various safety standards which ship engineers are required to follow. It is therefore necessary to consider a ship's safety during its initial design stages. The larger ships such as large cargo carriers require strict safety standards. With larger vessels such as these, the IMO safety standards stipulate the need for a vessel to demonstrate high maneuverability – this may be achieved with a twin-screw ship. Demand for twin-screw ships will therefore increase in near future. Thus, when it comes to the maneuverability of a twin-screw ship, the existing research leaves a lot to be desired as it primarily focuses on container ships. For these reasons, it is crucial that thorough research is performed on the maneuverability of other styles of twin-screw ships, such as naval combatants.

Most studies on the manoeuvrability of twin-screw ships have focused on container ships as there is an abundance of existing data available for them. However, container ships tend to have less manoeuvring problems compared to other types of ships. Thus, when it comes to the manoeuvrability of a twin-screw ship, the existing research leaves a lot to be desired as it primarily focuses on container ships. For these reasons, it is crucial that thorough research is performed on the manoeuvrability of other types of twin-screw ships, such as naval combatants.

The main goal of this research is to assess the manoeuvrability of the twin-screw naval combatant ship the DTMB 5415 using Computational Fluid Dynamics (CFD) and MATLAB. In this research, Star-CCM+ is used as a RANS solver to measure the hydrodynamic forces and moments on the twin-screw and derive the hydrodynamic derivatives. To validate the simulated results, a comparison is made against the existing experimental data from the published literature. Following this, MATLAB will be used to predict the manoeuvrability of the vessel in question such as its turning ability and course changing ability. A Mathematical Modelling Group (MMG) model is then used to predict the individual hydrodynamic forces of the propeller and hull.

Keywords: Manoeuvrability, CFD, MMG model, naval combatants

TABLE OF CONTENTS

List of Table

List of Figure

1 Introduction

1.1 General remarks

The International Maritime Organization (IMO) has proposed various safety standards which ship engineers are required to follow. It is therefore necessary to consider a ship's safety during its initial design stages. In particular, the larger ships such as large cargo carriers require strict safety standards. With larger vessels such as these, the IMO safety standards stipulate the need for a vessel to demonstrate high maneuverability – this may be achieved with a twin-screw ship. Demand for twin-screw ships will therefore increase in near future. Thus, when it comes to the maneuverability of a twin-screw ship, the existing research leaves a lot to be desired as it primarily focuses on container ships. For these reasons, it is crucial that thorough research is performed on the maneuverability of other styles of twin-screw ships, such as naval combatants.

Recently, vessels are becoming larger in size to maximise the benefit. Because of building bigger ships, the damage when a ship gets in an accident is also more critical. It is necessary to consider the safety regulation from the basic design stage.

Generally, a twin-screw ship's manoeuvrability is superior compared to the single-screw's one. (Will, et al., 2013) In addition, it is well known that a twin-screw ship has the better Fuel Oil Consumption (FOC) than a single-screw ship's one. (MAN Diesel & Turbo, 2007) It means that a twin-screw ship maintains the propulsion with less fuel oil consumption than a typical single-screw ship.

1.2 Scope

In this study, the DTMB 5415, twin-screw ship which was used as a benchmarking vessel in SIMMAN 2008 and SIMMAN 2014 workshops is chosen as a target vessel. The hydrodynamic forces and moment is calculated using Computational Fluid Dynamics (CFD). It is difficult to perform full experimental test according to the IMO maneuverability standards. Also, the Planar Motion Mechanism (PMM) test needs expensive equipment and technical constraints. For this reason, CFD is used to conduct PMM test. Star CCM +, a commercial CFD software, is used to obtain hydrodynamic derivatives.

Following this, a Simulink model is structured according to Mathematical Modelling Group (MMG) model. There are two types of Simulink model. First one is 35° turning simulation for predicting turning ability and the other is zigzag simulation model in order to predict course changing ability. The hydrodynamic derivatives obtained from STAR-CCM+ is stored on the M-file which is a function of MATLAB. Those derivatives are used when the Simulink models are executed.

At the last step of this study, it is expected that turning ability are predicted through 35° turning simulation as well as predicted course changing ability by conducting 10/10, 20/20 zigzag simulation

This thesis is organised as follows: Chapter 2 is a critical review section. In Chapter 3 the methodology employed in this study is explained. Next, the results are presented in Chapter 4. Finally, Chapter 5 is about conclusion and future work.

1.3 Aims and objectives

Compared to physical experiments, Computational Fluid Dynamics is financially efficient, and the intensity of physical labour is also low. However, there has been a drawback that it is difficult to equip computer hardware to perform large capacity calculations. But recently with the development of computer hardware technology, the value of CFD is increasing. In this study, the accuracy of CFD calculations was validated by comparing CFD calculations with

the existing experimental data. After conducting CFD calculation, the obtained derivatives applied on Simulink structure which is based on MMG model. Using this model, turning ability and course changing ability are predicted. The specific objectives of this research study are as follows.

(1) To Perform Virtual Captive Model Test to validate the accuracy of CFD.

(2) To construct a MMG model to simulate maneuver tests utilising Matlab/Simulink.

(3) To predict the maneuverability characteristics of the ship in question

2 Critical Review

2.1 Introduction

In this chapter, the findings of a background study on ships manoeuvrability problems are presented with a view to providing an overview of the research that has been carried out in this field.

2.2 Maneuverability

International Maritime Organization (IMO) has suggested the standards for maneuverability tests (Daidola, et al., 2002). According to these standards, a turning test is to be performed with 35° rudder angle (both starboard side and port side). The advance distance should not exceed 4.5 ship lengths (L) and tactical diameter should not exceed 5 ship lengths. Advance distance is defined as how much the ship advances until the heading angle is 90°. Tactical diameter is lateral distance until the heading angle is 180°. When it comes to zig-zag tests, there are 2 sorts of tests. These are 10°/10° zig-zag test and 20°/20° test. When 10°/10° zig-zag test is conducted, the first overshoot angle should not be more than 15°. In same way, the first overshoot angle in 20°/20° zig-zag test should not be over 25°.

The SIMMAN workshop was held twice in 2008 and 2014 to discuss the verification and validation of ship manoeuvring simulation methods. SIMMAN 2014 was held (Otzen & Simnonsen, 2014). As following current trend, much more research using CFD was presented in various areas such as manoeuvrability in in shallow water and in wave conditions. The benchmarking vessels for this workshop were the KVLCC2, the KCS and the DTMB 5415.

Lee et al. (1997) investigated the mathematical models in the case of twin-skeg ship. The main subject was propeller effective wake and effective neutral rudder angle δ_R. Mathematical model of maneuvering for a single-skeg ship had developed. But, Mathematical model in terms of twin-skeg has not studied sufficiently because it is not popular type. In this situation, he calculated simulated maneuverability using the twin-skeg simulation model.

Kim et al. (2006) conducted PMM (Planar Motion Mechanism) tests for obtaining hydrodynamic derivatives and hull-rudder interaction coefficients. In that research, 4 DOF (Degree of freedom) MMG was applied and the target vessel is 12,000 TEU container ship which is a twin-screw model. The maneuvering simulation was carried out using derived derivatives and coefficients. In this simulation, the flow straightening coefficient (γ_R) changed according to drift angle. The reason why Kim et al. used this technic was two rudders have different straightening coefficients in turning test. In order to consider this situation, different coefficients according to drift angle were used. Consequently, in this study, it was considered the interaction between rudders through changing straightening coefficients.

PMM test with 5.72 m DDG 51 frigate model, which is 24.830 scale naval combat, was performed (Benedetti et al, 2007). In this report, the uncertainty analysis has been conducted for PMM test and it has been applied on three static and five dynamic tests. 3 DOF was applied. The results, such as surge force, sway force, yaw moment, were compared with the experimental data. Not only conducting CFD simulation but also four types of model tests are carried out which cover pure drift, static test, and three dynamic tests; Pure sway, Pure yaw, Yaw and drift test. Surge force and sway force, yaw moment was measured through PMM test. 4 types of test were conducted such as static drift, pure sway, pure yaw, yaw with drift test as matched with CFD simulations.

Yoon (2009) conducted PMM test for obtaining hydrodynamic derivatives. As well as simulated the virtual captive model tests using CFD. In this research, uncertainty analysis was conducted to estimate the accuracy of the tests. Flow fields were observed in pure sway and pure yaw CFD simulation.

2.3 Validation of computational fluid dynamics

Phillips et al. (2007) performed PMM tests using a scale model of the Autonomous Underwater Vehicle (AUV) Autosub using unsteady Reynolds-averaged Navier-Stokes (RANS) simulations to obtain its hydrodynamic derivatives. In their study they used the overset mesh to observe the unsteady flow. This mesh moves relatively unlike a fixed outer domain. In this paper, detail results for pure sway motion were presented and the results showed the cost of computational analysis was appropriate. It was used as a prediction data at the initial design stage with a full set of manoeuvring derivatives.

Zou et al. (2010) conducted a verification and validation study of CFD simulations for a KVLCC2 tanker with bare hull model. The simulations were performed for varying drift angles and water depths. A steady state Reynolds Averaged Navier-Stokes solver was applied to solve the viscous and the free surface, sinkage and trim are ignored. Uncertainty analysis was also performed in terms of hydrodynamic forces and moments which were estimated through grid convergence studies and discretisation errors were calculated. Validation was performed by comparing with experimental data. Summary, a technique to predict the numerical uncertainty and for the validation and verification accuracy of CFD had applied to a tanker at various drift angles and water depths.

Simonsen et al. (2012) performed PMM test with appended model ship and Virtual Captive Model Test based on IMO manoeuvring simulations. Computed hydrodynamic derivatives and measured input data were used for maneuvering simulations. The standard 10/10 and 20/20 zigzag and the 35 turning circle maneuvers were simulated. All PMM conditions were computed using STAR-CCM+ in order to calculate hydrodynamic forces and moments. Comparison between the computed and measured forces and moments showed a reasonably

good agreement. The result showed that the surge force agrees well with the experiments, whereas the sway force and the yaw moment did not.

Oldfield and Larmaei (2015) conducted virtual captive model test using CFD for verification and validation of maneuvaring simulation. Through conducting static drift, pure sway, pure yaw, yaw with drift tests and rotating arm test, X, Y forces and N moment were measured, and hydrodynamic derivatives were also obtained. These data were used for validation in this paper. Wave pattern near the model ship were observed in steady and unsteady simulations.

Tezdogan et al. (2015) carried out a validation study using CFD and the target vessel was a full-scale ship of the KRISO Container Ship appended with a rudder. Through the resistance test, a fully nonlinear unsteady RANS simulation to predict the ship motions and added resistance was performed in regular head waves. Their simulated results were validated against experimental data and compares with the results from potential theory.

Dash and Nagarajan (2015) conducted an uncertainty study for mathematical model using the DTMB 5415. The uncertainty of the mathematical model was found to be higher than the experimental uncertainty. The uncertainty analysis results will be useful for improving of mathematical model and validation of CFD simulation results.

Yasukawa and Yoshimura (2015) introduced MMG standard method. In their article, the virtual captive model test such as Rudder force test in straight moving under various propeller loads and Oblique towing test (OTT) and circular motion test (CMT) and Rudder force test in oblique towing and steady turning conditions (flow straightening coefficient test) are conducted in order to obtain hydrodynamic derivatives and rudder-propeller interaction coefficients. Using these derived coefficients, turning and zig-zag simulations were carried out. The accuracy was validated by comparing with experimental results.

Hajivand and Mousavizadega (2015) performed maneuvering oblique towing test in a numerical towing tank to obtain the linear and nonlinear velocity dependent damping coefficients for a model ship. The simulations were conducted in accessible OpenFOAM library with three different solvers which were rasInterFoam, LTSInterFoam and interDyMFoam, with two turbulence models, k-ε and SST k-ω, in presence of free surface. Turning and zigzag simulations were calculated for the DTMB 5512 model ship using the

derived damping coefficients from CFD. The simulation results were compared with the available experimental data.

The research in terms of hull-propeller-rudder interactions using CFD also carried out not only PMM. Duman and Sezen (2017) conducted hydrodynamic analyses at a relatively higher Froude number using unsteady RANS approach. The surface combatant DDG51 in 1:46.588 scale which is known as the DTMB5512 is fixed during the analyses. In their paper, Duman and Sezen (2017) investigated the open water hydrodynamic performance of the propeller and the pressure distributions on the hull surface as well as the wave elevations in the wake. They also looked at the change in the drag coefficient with and without the rudder/propeller. They also compared their computational results with the experimental ones. After validation, twin-rudder and twin-inward-propeller have been implemented.

2.4 Summary

As can be seen from this literature review, CFD tools are becoming more popular for use in connection with ship manoeuvrability problems. For this reason, a commercial CFD software package (Star-CCM) was used in this study to calculate the hydrodynamic forces and moments to estimate the hydrodynamic derivatives of the ship in question.

3 Methodology

3.1 Introduction

Overall, this study is divided into two parts. The first part is the Virtual Captive Model Test. Four types of Virtual Captive Model Experiments were performed: Static Drift, Pure Sway, Pure Yaw, and Yaw with Drift. Through these simulations, the hydrodynamic derivatives were calculated through the measured forces and moment. The second part is the MMG Model. To predict the turning ability and course changing ability of a ship, the hydrodynamic derivatives were stored on m-file (script) of MATLAB and then the simulation performed using the 3-DOF MMG model built by Simulink. By using these procedures, the maneuverability of the ship was predicted.

3.2 Maneuvering Equation of MMG model

In this study, a MMG model was used. The MMG model considers the hydrodynamic forces and moment acting on the ship by dividing it into the hydrodynamic forces and moment acting on the hull, the hydrodynamic forces and moment acting on the propeller, and the hydrodynamic forces and moment acting on the rudder. Therefore, in this study, the mathematical model of maneuvering Equation was constructed by dividing the forces and moment into three parts.

3.2.1 Coordinate system

In the present study, it is considered that the ship is navigating in the calm water. The motions of a ship are defined for only planar motion, namely Surge, Sway and Yaw. Also, the Earth fixed coordinate system and the ship fixed coordinate system are used as shown in Figure. 1. When estimating the maneuverability of the ship, it is easy to measure the tactical diameter, advanced distance and transfer distance for turning ability by using the earth fixed coordinate system. However, when calculating the hydrodynamic force acting on the ship, it is convenient to express using the ship fixed coordinate system. Therefore, the research is

conducted using the coordinate system $O-xyz$ which is fixed on the mid-ship as shown in the Figure. 1.

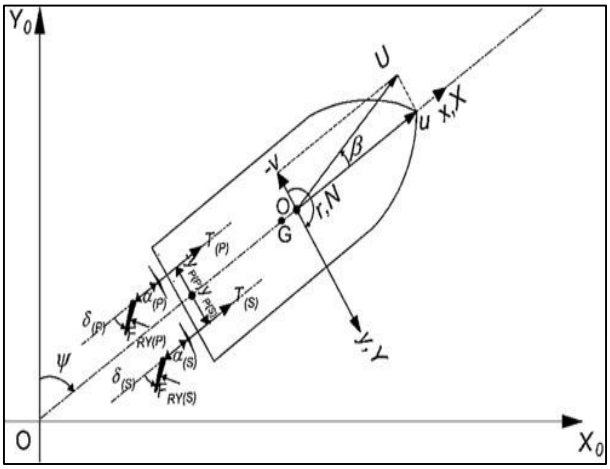

Figure 1. Coordinate system

The surge force is X, the Sway force is Y, and the moment in Yaw direction is N in the ship fixed coordinate system. When it comes to the earth fixed coordinate system, the $X_0 - Y_0$ plane is located on the water surface, and the Z_0 axis has the positive (+) direction when it goes down. The drift angle is defined as β, where $\beta = \tan^{-1}(-\frac{v_M}{u})$. The starboard direction rudder angle is defined as $\delta(s)$, and the port direction rudder angle is defined as $\delta(p)$. The angle between the X_0 axis and the x axis is defined as the heading angle (ψ). The velocity of the ship is defined as $U\ (=\sqrt{u^2+v_m^2})$, the velocity in the x direction is defined as u, the velocity in the y direction is defined as v and the angular velocity in the clockwise direction is defined as r.

In this study, the origin is fixed on the mid-ship rather than the centre of mass in the ship fixed coordinate system. The reason for this is that the centre of mass can be changed according to the loading condition and the distance between the origin of the coordinate system and the distance to the propeller and rudder changes at the same time.

To express a mathematical model based on these coordinate systems, the following assumptions have been made:

(1) A ship is a rigid body whose shape is not changed by external force.

(2) The ship is floating on calm water

(3) The hydrodynamic forces acting on the ship are considered as quasi-steady forces.

(4) The lateral velocity is relatively small compare to the longitudinal velocity.

(5) The effect of roll motion acting on the ship is ignored, since the metacentric height (GM) is large enough.

3.2.2 Maneuvering Equation

In the present study, the maneuver equation is expressed on the horizontal plane. The Surge, Sway forces and Yaw moment acting on the ship are expressed using the Euler Equation as shown in the following Equation (1).

$$\begin{aligned} F_x &= m(\dot{u} - vr) \\ F_y &= m(\dot{v} + ur) \\ M_z &= I_{zG}\dot{r} \end{aligned} \tag{1}$$

m is the mass and I_{zG} is inertia of the ship relative to the z axis. u, v, r are unknown variables. When it comes to the maneuver, u is forward speed and v is lateral speed. Also, r is defined as the yaw rate. And also, F_x, F_y and M_z can be expressed as below Equation (2).

$$\begin{aligned} F_x &= -m_x\dot{u} + m_y v_m r + X \\ F_y &= -m_y\dot{v}_m - m_x ur + Y \\ M_z &= -J_z\dot{r} + N_m - x_G F_y \end{aligned} \tag{2}$$

The added masses on the x and y axises are represented by m_x and m_y, respectively, and J_z is added moment of inertia. Since this study was not carried out in the origin of centre of mass but instead at the origin of the mid-ship, the relation Equation between the lateral velocity at the centre of mass and the lateral velocity at the mid-ship is substituted. When the origin of centre moves further forward than the origin of the mid-ship, the relation is expressed as below in Equation (3).

$$v = v_m - x_G r \tag{3}$$

Equation (4) is derived from Equation (1), (2) and (3). Equation (4) has its origin at the mid-ship.

$$\begin{aligned}(m+m_x)\dot{u}-\left(m+m_y\right)v_m r-x_G m r^2 &= X\\ \left(m+m_y\right)\dot{v_m}+(m+m_x)ur+x_G m\dot{r} &= Y\\ (I_{zG}+x_G^2 m+J_z)\dot{r}+x_G m(\dot{v}_m+ur) &= N_m\end{aligned} \tag{4}$$

Equation (4) must be solved to estimate the maneuverability of a ship. In terms of MMG (Mathematical Modelling Group) model, X, Y forces and N moment is divided into three parts as in Equation (5).

$$\begin{aligned}X &= X_H+X_P+X_R\\ Y &= Y_H+Y_P+Y_R\\ N_m &= N_H+N_P+N_R\end{aligned} \tag{5}$$

The subscript H means the hydrodynamic force by hull, P and r are the hydrodynamic force and moments due to the propeller and the rudder, respectively. When the influence of the propeller on y force and N moment are negligible, Equation (5) is reduced to Equation (6) as follows:

$$\begin{aligned}X &= X_H+X_P+X_R\\ Y &= Y_H+Y_R\\ N_m &= N_H+N_R\end{aligned} \tag{6}$$

3.2.3 Hydrodynamic force acting on the hull

The hydrodynamic force acting on the hull can be expressed as below in Equation (7).

$$\begin{aligned}X_H &= \frac{1}{2}L_{PP}dU^2X'_H\,(\mathrm{v}'_\mathrm{m},\mathrm{r}')\\ Y_H &= \frac{1}{2}L_{PP}dU^2Y'_H(\mathrm{v}'_\mathrm{m},\mathrm{r}')\\ N_H &= \frac{1}{2}L_{PP}^2dU^2\mathrm{N}'_\mathrm{H}(\mathrm{v}'_\mathrm{m},\mathrm{r}')\end{aligned} \tag{7}$$

where ρ is the density of water, L_{PP} is the distance between the after perpendicular and front perpendicular, d is the draft, and U is the ship speed. The prime in Equation (7) indicates a non-dimensional term, that is, it is assumed that the forces are divided by $\frac{1}{2}\rho dU^2$. v_m is the lateral velocity in the mid-ship and v_m' is v_m/U. r represents the angular velocity, and it is with r' is rL_{PP}/U. X_H, Y_H and N_H are expressed as polynomials of v_m and r using Taylor series expansion. Equation (8) illustrates this in more detail.

$$\begin{aligned} X_H'(v_m', r') &= -R_0' + X'_{vv}v_m'^2 + X'_{vr}v_m'r' + X'_{rr}r'^2 + X'_{vvvv}v_m'^4 \\ Y_H'(v_m', r') &= Y_v'v_m' + Y_r'r' + Y'_{vvv}v_m'^3 + Y'_{vvr}v_m'^2r' + Y'_{vrr}vr'^2 + Y'_{rrr}r_m'^3 \\ N_H'(v_m', r') &= N_v'v_m' + N_r'r' + N_{vvv}v_m'^3 + N'_{vvr}v_m'^2r' + N'_{vrr}vr'^2 + N_{rrr}r_m'^3 \end{aligned} \quad (8)$$

Here, $X_{vv}, Y_v,$ etc. are partial differential form such as $\frac{\partial X}{\partial vv}, \frac{\partial Y}{\partial v},$ etc. These are called as the hydrodynamic derivatives. When it comes to X Taylor expansion, it is even function. Whereas, Y force and N moment expansions are odd function. Because, a ship is bilateral symmetry. Therefore, even terms in X force's Taylor expansion and odd terms in Y force, N moment's expansions are ignored.

3.2.4 Hydrodynamic force acting on the propeller

The principle dimensions of the propeller are provided in Table 1.

Table 1. Propeller characteristic

Characteristic	Value
Number of blade	5
Hub ratio	0.16
Diameter	6.15(m)

Since the hydrodynamic force generated by the propeller mainly affects the surge motion, the terms for sway force (Y_p) and yaw moment (N_p) can be ignored. The hydrodynamic force by the propeller can be expressed in Equation (9)

$$X_p = (1 - t_P)T \tag{9}$$

In the above Equation, t_P is the thrust deduction coefficient and T is the thrust. The thrust deduction coefficient represents the rate of increase in resistance because a propeller is located at the stern. T is expressed as below in Equation (10).

$$T = \rho n_P^2 \mathrm{D_P^4} K_T(J_P) \tag{10}$$

Where ρ is water density. The n is revolutions per minute of a propeller. D_P is the diameter of propeller and K_T is a function of J_P. The J_P is propeller advance coefficients. K_T is expressed as a polynomial Equation, and the coefficient k_0, k_1, k_2 can be estimated for the polynomial Equation from the propeller open water test results. The Equation of K_T is as below Equation (11).

$$K_T(J_P) = k_2 J_P^2 + k_1 J_P + k_0 \tag{11}$$

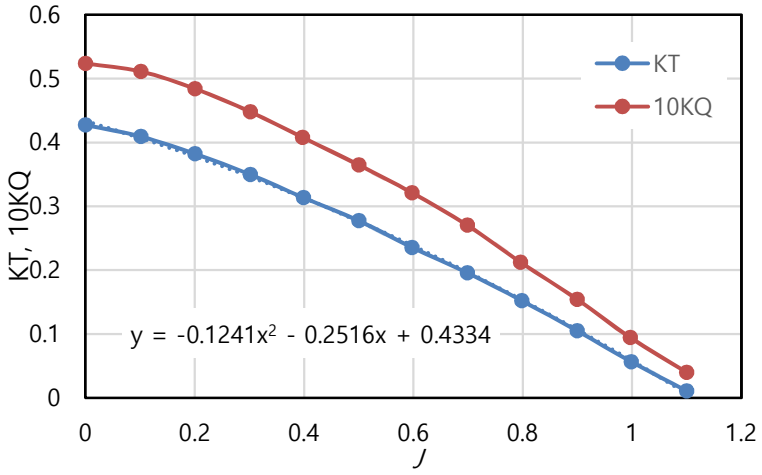

Figure 2. Propeller open water data

k_0, k_1 and k_2 are estimated using the propeller open water data from SIMMAN 2014 (Otzen & Simnonsen, 2014) as shown in Figure 2. Thus, It is estimated that $k_0 = 0.4334$, $k_1 = -0.2516$, $k_2 = -0.1241$. At this point, $\mathrm{J_P}$ is described as follows in Equation (12).

$$J_P = U(1 - w_p)/n_P D_P \tag{12}$$

The w_p is the wake coefficient and it is estimated from the Equation (13).

$$\begin{aligned} w_P &= w_{P0}\exp\{-C_P v_P^2\} \\ v_P &= v + x_P r \end{aligned} \tag{13}$$

$w_{p0}$is the wake coefficient from propeller Open Water Test. The x_P is the longitudinal direction position of the propeller. In the Simulink simulation of this study, the wake coefficient and thrust reduction coefficient are quoted. w_P is 0.031 and t_P is 0.095 for the propeller in question.

3.2.5 Hydrodynamic force acting on the rudder

In the case of the hydrodynamic force with respect to the rudder, it is expressed using the rudder normal force, F_N. This is because the lift force can change even when the hull moves a little, but in the case of the rudder normal force, it is defined uniformly according to the angle of attack incident on the rudder. The rudder tangential force is negligible since it is very small. The hydrodynamic force by the rudder is expressed in Equation (14)

$$\begin{aligned} X_R &= -(1 - t_R)F_N sin\delta \\ Y_R &= -(1 + a_H)F_N cos\delta \\ N_R &= -(x_R + a_H x_H)F_N cos\delta \end{aligned} \tag{14}$$

The t_R is the steering resistance deduction factor due to interaction between the hull and the rudder. The x_R is the longitudinal coordinate of rudder position. The x_H is the longitudinal coordinate of acting point of the additional lateral force. δ is rudder angle. The longitudinal force generated by the rudder and hull interference is regarded as an increase in resistance. It is considered in X_R term using t_R. Circulation is also induced in the hull when the rudder moves.

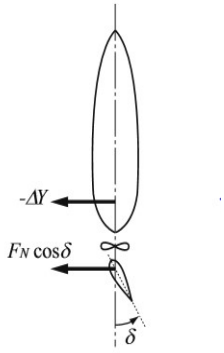

Figure 3. Induced Lateral Force by steering

There is circulation around the rudder when the rudder is steered on the stern. This circulation also affects the hull and induces the lift force acting on the hull. In Figure 3, when the rudder is steered, the lift force occurs on the rudder, and circulation occurs around the rudder at the same time. This circulation also affects the hull and induces the lift force ($-\Delta Y$) on the hull. Therefore, the lift force that acts on the hull due to the steering is expressed as in Equation (15).

$$\begin{aligned} Y_R &= -F_N \cdot cos\delta - \Delta Y \\ N_R &= -F_N \cdot cos\delta \times x_R - \Delta Y \times x_H \\ \Delta Y &= a_H \cdot F_N cos\delta \end{aligned} \tag{15}$$

The a_H is the rudder force increase factor. The added Y force induced by steering is a_H times compared to Y force acting on the hull. Therefore, Equation (15) change to Equation (16)

$$\begin{aligned} Y_R &= -(1 + a_H)F_N cos\delta \\ N_R &= -(x_R + a_H \cdot x_H)F_N cos\delta \end{aligned} \tag{16}$$

Here, the rudder normal force F_N is expressed as in Equation (17).

$$F_N = (1/2)\rho A_R U_R^2 f_\alpha sin\alpha_R \tag{17}$$

The variables included in the above Equation are derived as in Equation (18).

$$U_R = \epsilon u_P \sqrt{\eta \left\{ 1 + k \left(\sqrt{1 + \frac{8K_T}{\pi J_P^2}} - 1 \right) \right\}^2 + (1 - \eta)} \tag{18}$$

$\rightarrow \ \eta = \frac{D_P}{H_R},\ \alpha_R = (\delta - \delta_0) - \gamma_R (v' + l_R r')(\frac{U}{u_R}),\ l_R \cong 2x_R$

The thrust is increased due to the lift force generated by the rudder, but this phenomenon is expressed by introducing a coefficient of $(1 - t_R)$ in consideration of the decrease in resistance. The x_R is the x position of the rudder. The D_P, H_R are the diameter of the propeller and the height of the rudder, respectively.

However, since the target ship is a twin-screw in the present study, it is necessary to modify the above the maneuvering Equations to be proper for a twin-screw ship. The maneuvering equations of the twin-screw ship are expressed by dividing into the port-side rudder and the starboard-side rudder; see Equation (19.

$$\begin{aligned} X_R &= X_R^P + X_R^S \approx -(1 - t_R)\left(F_N^P + F_N^S\right) sin\delta \\ Y_R &= Y_R^P + Y_R^S \approx (1 + a_H)\left(F_N^P + F_N^S\right) cos\delta \\ N_R &= N_R^P + N_R^S \approx (x_R + a_H x_H)\left(F_N^P + F_N^S\right) cos\delta - y_R(1 - t_R)\left(F_N^P - F_N^S\right) sin\delta \end{aligned} \tag{19}$$

The coefficients of interferences due to the rudder and the hull of the twin-screw are expressed using Equation (20).

$$\begin{aligned} \gamma_R^P \ at \ \beta_R &= \gamma_R^S \ at - \beta_r \\ \delta_0^P &= -\delta_0^S \\ \epsilon^P = \epsilon^S, \qquad k^P &= k^S \end{aligned} \tag{20}$$

In this study, the maneuvering forces acting on the hull were derived by using the commercial CFD (Computational Fluid Dynamics) software, STAR-CCM +, and the propeller open water test data using the force technology data published by SIMMAN 2014.

3.3 Virtual captive model test

3.3.1 Test matrix

The recommendation and guideline has discussed in International Towing Tank Conference (ITTC, 2017). ITTC suggested recommended procedures and guidelines. In this procedure, there is a guideline part for maneuvering using CFD. It is 'Guideline on Use of RANS Tools for Manoeuvring Prediction (2017)'. In this guideline, there are specific recommendations when conducting maneuvering simulations for scale, turbulence model, propulsion model, computational grid, boundary conditions, free surface treatment. In this paper, virtual captive model test and analysis are conducted following this guideline as example.

In this study, the Virtual Captive Model Test is conducted using STAR-CCM+, a commercial CFD (Computational Fluid Dynamics) software. The test matrix for simulations and the derived coefficients are shown in Table 2 below. Froude number is 0.28, 2.0965 *m/s* in this scale. In this study, the ship is free to pitch and heave since heave and pitch motions are important in planar motion mechanism tests. Table 2 shows the model test conditions as in the SIMMAN 2014 specification.

Table 2. Virtual captive model test condition

Simulation Type	Variable/Condition	Derivatives
Static Drift	β (Drift angle)/ $0°, 2°, 6°, 9°, 10°, 11°, 12°, 16°, 20°$	$X_{vv}, Y_v, Y_{vvv}, N_v, N_{vvv}$
Pure Sway	v'(Sway velocity)/ 0.03, 0.07, 0.17	$Y_{\dot{v}}, N_{\dot{v}}$
Pure Yaw	r'(Yaw velocity)/ 0.05,0.15, 0.30, 0.45, 0.60, 0.75	$X_{rr}, Y_r, Y_{rrr}, N_r, N_{rrr}, Y_{\dot{r}}, N_{\dot{r}}$
Yaw with Drift	β(Drift angle)/ $9°, 10°, 11°$ r'(Yaw velocity)/ 0.03	$X_{vr}, Y_{vvr}, Y_{vrr}, N_{vvr}, N_{vrr}$

3.3.2 Target vessel

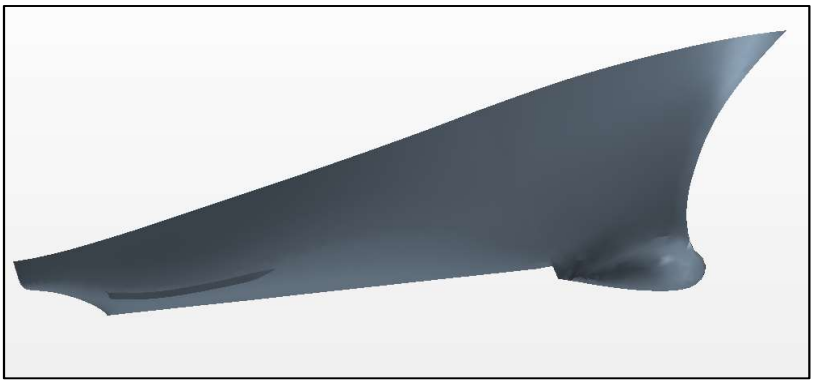

Figure 4. The DTMB 5415 bare hull with bilge keels

In the present study, the DTMB 5415 was chosen as a target vessel which is illustrated in Figure 4. The DTMB 5415 was a target vessel in the SIMMAN 2008 and SIMMAN 2014 workshops. Therefore, the result of the hydrodynamic derivatives from the model tests of the DTMB 5415 are publicly available. That is the one of the reasons why the DTMB 5415 was chosen. The CAD model for the bare hull and the bilge keels on the SIMMAN 2014 website were used in this study. The CAD file of ship was repaired using STAR-CCM+. It is used as validate data in this study. Bare hull with bilge keels model, which is 1:24.83 scale, was used in this study. The main dimensions of the DTMB 5415 are defined in Table 3. The target vessel has two propellers and rudders. It means that the mathematical equations are different from those for a single screw. To consider this, modified mathematical Equations were applied. This study has been investigated using unsteady RANS (Reynolds-averaged Navier-Stokes).

Table 3. Principle dimension of the DTMB 5415

Characteristic	Full scale	Model scale
Scale	1	24.830
$L_{pp}(m)$	142	5.719
$B_{wl}(m)$	19.06	0.768
$d(m)$	6.15	0.248

$\nabla(\mathrm{m}^3)$	84244	0.554
$x_G(\mathrm{m})$	-0.652	-0.026
C_B	0.507	0.506
$S\ w/o$ rudder (m^2)	2972.6	4.861

3.3.3 Physical modelling and numerical setup

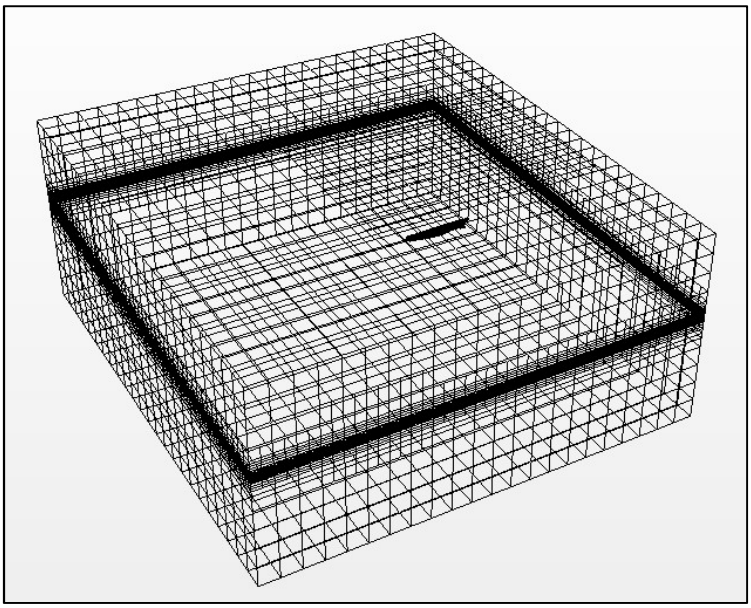

Figure 5. Computational domain

Table 4. Virtual towing tank size

Longitudinal	39.5 (7L)	m
Lateral	43.2 (7.56L)	m
Vertical	18 (3.15L)	m

Figure 5 shows the computational domain which is used in this study and Table 4 shows the dimensions of the computational domain. The size of the computational domain for maneuvering simulation was decided as following the recommendations of the ITTC 2017 procedure (2017). The domain was generated with a size corresponding to 7 times of L_{pp} in

the longitudinal direction of the ship, 7.56 times of L_{pp} in the horizontal direction and 3.15 times of L_{pp} in the vertical direction in accordance with the above-mentioned ITTC Procedure. The domain size, in this study, was intentionally taken slightly bigger than the recommended distances. The reason for this was that the domain size which is advised in the ITTC procedure is not enough to adequately capture Kelvin waves. 1.5 million cells have been recommended as the minimum acceptable amount of a grid and a grid of 4 million cells is suggested for an optimum grid (Simonsen, 2012). In this study, for efficiency, grid of 1.8 million cells was used.

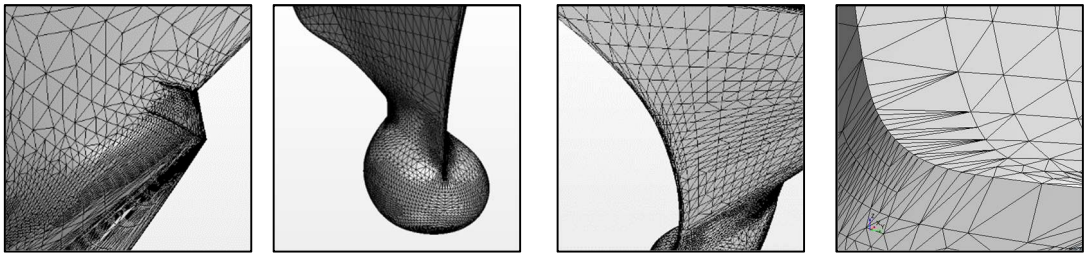

Figure 6. Surface mesh

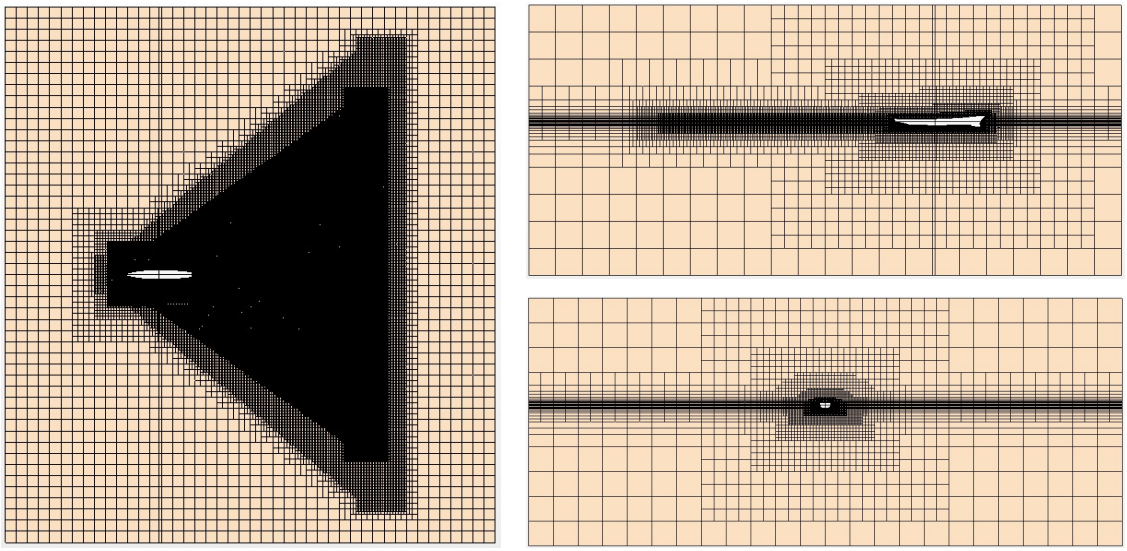

Figure 7. Volume mesh

The surface mesh of the hull and the space lattice were made of a trimmed mesh shown in Figure 6 and Figure 7. By using the trimming lattice method, the lattice structure and density are different according to the flow characteristics. It means that the size of mesh is set relatively small for the complex flow region and the mesh size is set large for the simple flow

region. The prism layers are generated on the near hull where shear force is important. The prism layers are used to accurately measure the boundary layer flow on the hull surface and generated totally six prism layers from the hull surface. The thickness of the entire boundary layer is defined as the value derived from the boundary layer thickness Equation (21) for the plate.

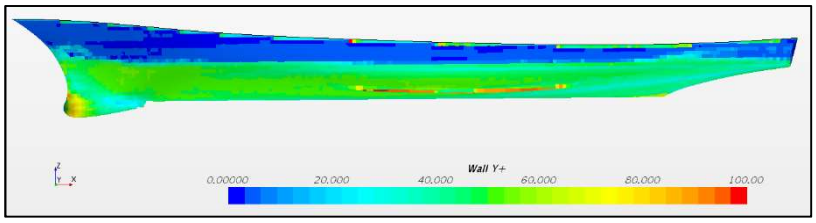

Figure 8. y+ Scene applied two-layer y+ solver

$$\frac{\delta}{x} = 0.382\left(\frac{\nu}{Ux}\right)^{\frac{1}{5}} = \frac{0.382}{Re_x^{\frac{1}{5}}} \tag{21}$$

For all the maneuvering simulations in CFD, the most important thing is to define the turbulence model, interface capturing, near-wall treatment, as well as boundary and initial conditions. A velocity inlet boundary condition was set in the positive x direction. The negative x direction was modelled as a pressure outlet. The top and bottom boundaries were both selected as velocity inlets. The side of the domain has a velocity inlet boundary condition as well. The velocity inlet is defined as the same flow as the ship's target speed. The outlet is defined the gradient to velocity and pressure to be zero. After generating boundaries, damping waves were applied on each boundary to prevent wave reflection from the walls. The length of damping waves was selected to be 1 L_{pp}.

When modelling a maneuver in CFD, the interface between the water and air can cause a huge error at high Froude numbers. A technique is required for capturing the interface in water surface. For this reason, multiphase flow was modelled using VOF (Volume of Fluid) method to position the free surface. Mainly, turbulence flow effects on the near wall. It means that the turbulence flow on the boundary layer influences the simulation results. For

considering this situation, in this study, a two-layer y+ was applied and simulations were modelled to be satisfied this condition. It is shown figure 8.

To complement the numerical simulation for the virtual captive model test. a Dynamic Fluid Body Interaction (DFBI) model employed. The DFBI model translates and rotates the entire computational domain to account for the dynamic attitude change of the hull. An implicit-unsteady solver was used for dynamic analysis of hull. The Realizable k-ϵ (RKE) turbulence model was used for numerical stability and efficiency.

Throughout this study's CFD word, the physical time was 45 seconds for each case. The reason for this is that, during the simulation, the vessel's motions converged after 15 seconds of physical time. After then, the motion was totally converging from 35 second. The time step was 0.015 seconds. The number of inner iterations was 10 per time step. The time step was calculated using the CFL number as below Equation (22).

$$CFL\ Number = \frac{u\Delta t}{\Delta x} \tag{22}$$

u is the magnitude of ship speed. Δt is the time step. Δx is the length of smallest mesh within the region. In this study, the size of time step was selected when CFL number is less than 1.

3.3.4 Grid convergence test

The grid convergence test was performed on the generated grid system before performing the virtual captive model. The grid convergence test was performed to find the optimal grid resolution for the grid system applied in Richardson extrapolation of the ITTC Recommended Procedure and Guideline. For this purpose, it was performed on three cases which are coarse, medium and fine grids for 20° static drift angle test. The three grids are determined by increasing the size of the grid with the refinement factor (r_i). At this time, the value of r_i is $\sqrt{2}$ following the ITTC Recommended Procedure and Guideline. The number of grids corresponding to the Coarse, Medium, Fine is shown in Table 5, and the generated grids are shown in Fig. 9.

Table 5. Reference size and number of grids

Index	Reference Size (m)	Number of grid
Coarse	0.1263	1,396,572
Medium	0.1125	1,839,055
Fine	0.1000	2,701,078

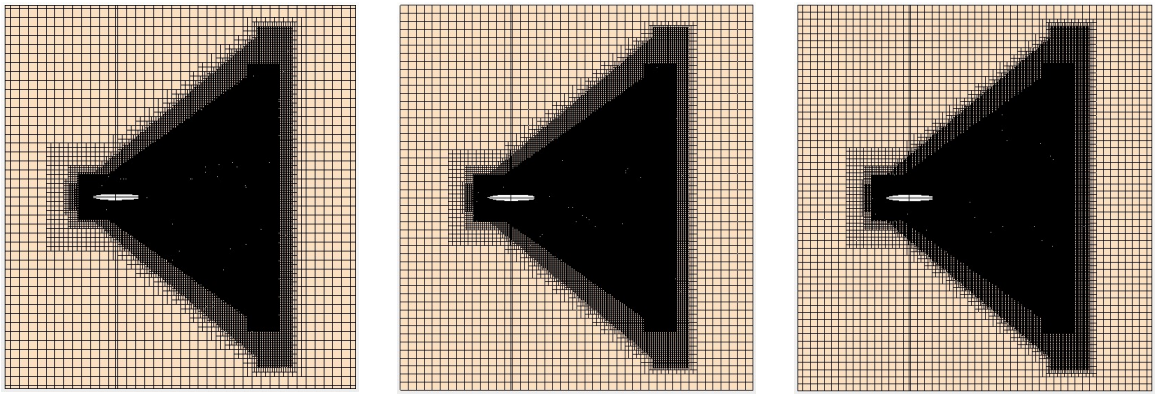

Figure 9. Different grids on top view (Coarse, Medium, Fine)

The differentece in the CFD results between Fine grid and Medium grid is $\epsilon_{i,12} = S_{i,2} - S_{i,1}$. The difference of Corse and fine grid is $\epsilon_{i,32} = S_{i,3} - S_{i,2}$. The convergence ratio is obtained by Equation (23) using the difference of the results.

$$R_i = \epsilon_{i,21}/\epsilon_{i,32} \tag{23}$$

Convergence condition is defined according to the convergence rate calculated by Richardson extrapolation as follows.

1) $R_i > 1$: Grid divergence

2) $R_i < 0$: Oscillatory convergence

3) $0 < R_i < 1$: Monotonic convergence

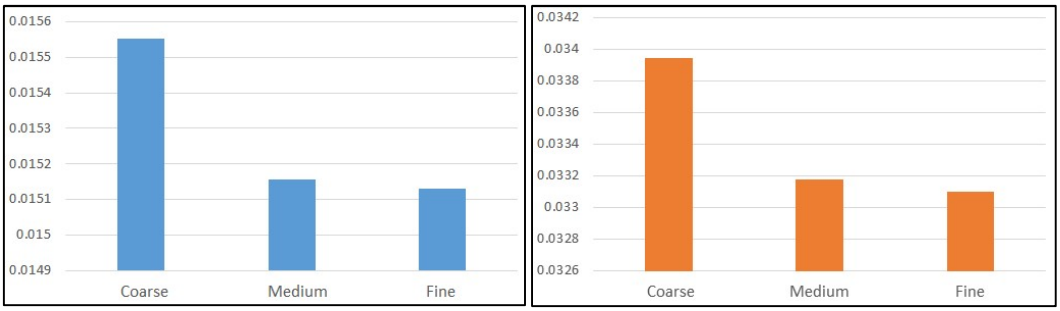

Figure 10. Surge force (Left) & Yaw moment (Right) related to grids

Figure 10 shows surge force and yaw moment according to grid number. The convergence rate and error are estimated as shown in Table 6 by using the non-dimensional surge force derived from the grid systems. The non-dimensionalization of the measured forces is performed as in Equation (24). The result of convergence test for surge force is shown in Table 6.

Table 6. Calculated convergence ratio of surge force

ϵ_{21}	ϵ_{32}	R_{G1}
2.59834E-05	0.000394005	0.065946962

R_{G1} for surge force is between 0 and 1 indicating a monotonic convergence. The non-dimensionalisation of the measured moment is performed in Equation (24). Yaw Moment was performed in the same manner. The results are shown in Table 7.

Table 7. Calculated convergence ratio of yaw moment

ϵ_{21}	ϵ_{32}	R_{G1}
8.22342E-05	0.000766716	0.107255073

R_{G1} for Yaw Moment is between 0 and 1. Both Forces and Moment are Monotonic convergence. It is shown that the tendency of calculated result converges as the size of the grid is reduced. Based on the efficiency such as the simulation time, this study conducted a virtual captive model test based on the grid size applied to the medium grid system.

4 Results

4.1 Static drift simulation

Static drift simulations for each drift angle were conducted at a constant towing speed U. This simulation was performed for a physical time of 45 seconds and the final 5 seconds average was used. The reason for this is that the ship's motion began to converge from the 15th second of the physical time and totally converge at 45th second.

Lateral velocity is defined as $v = -Usin\beta$. $X_0, X_{vv}, Y_v, Y_{vvv}, N_v, N_{vvv}$ are obtained using the definition of v and measured forces and moment from the Virtual Captive Model Test. Figures 11, 12, 13 and Table 8 show the results of Static Drift simulation compared with the experimental results from the study of Yoon et al. (2009). The model test, in Yoon et al.'s study, points the mid-ship as an origin, which is the same as the coordinate origin of the simulation performed in this study. The measured forces and moment in this study are shown in red dots, and the model test results are shown in black dots. Hydrodynamic derivatives are also compared with the experimental data.

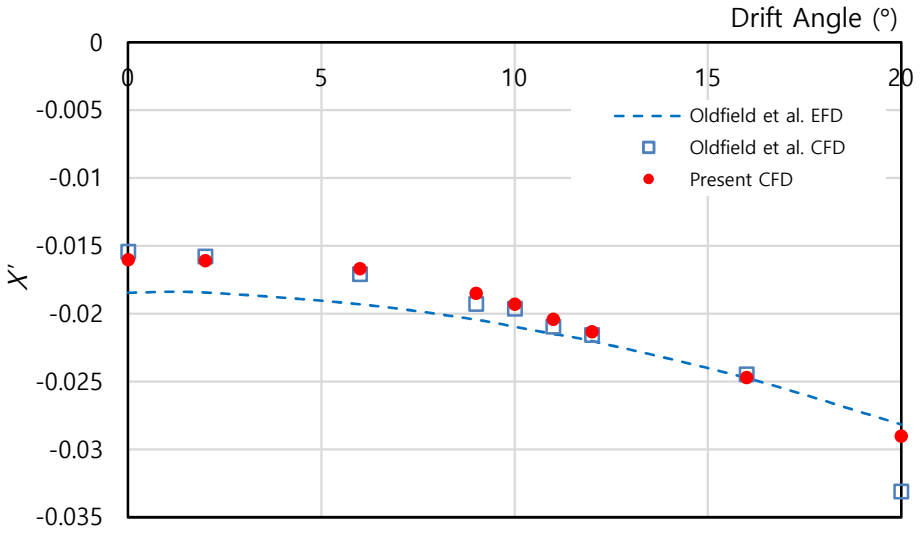

Figure 11. Non-dimensional surge force comparison in static drift

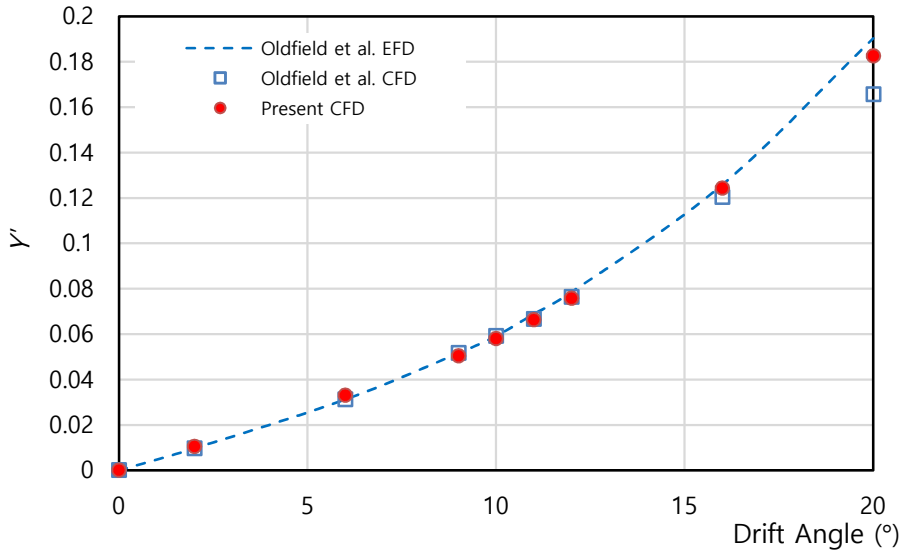

Figure 12. Non-dimensional sway force comparison in static drift

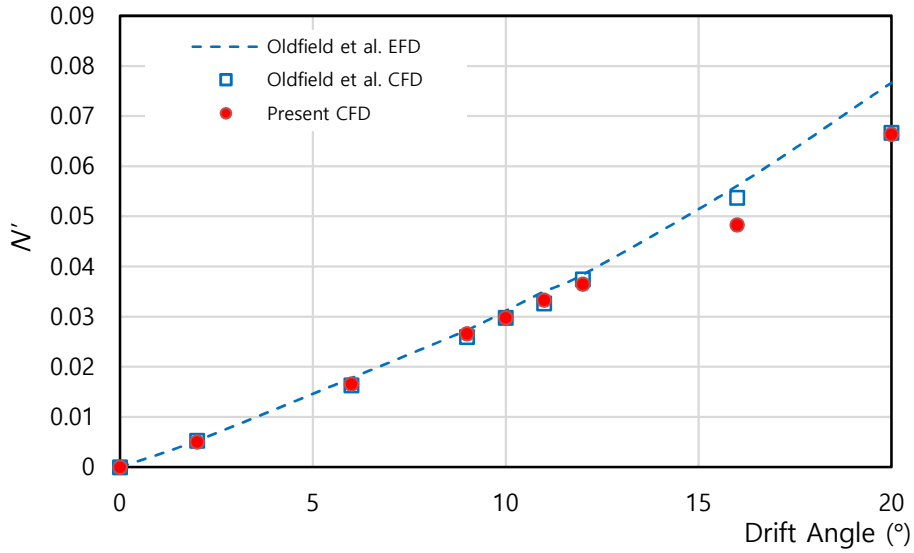

Figure 13. Non-dimensional yaw moment comparison in static drift

Table 8. Hydrodynamic derivatives in static drift simulation and comparison with the EFD data

Derivatives	Present CFD	EFD (Yoon et al., 2009)	Relative Error
$X_0{}'$	-0.01594	-0.0155	-2.84 %
$X_{vv}{}'$	-0.114	-0.1421	19.77 %
$Y_v{}'$	-0.2708	-0.3000	9.73 %
$Y_{vvv}{}'$	-2.265	-1.7875	-26.71 %
$N_v{}'$	-0.1615	-0.1628	0.80 %
$N_{vvv}{}'$	-0.2631	-0.3284	19.88 %

Post processing for calculating hydrodynamic derivatives, which is curve-fitted to polynomial functions, following Equation (26) were used.

$$y = A + Bx^2; y = X';\ x = v' \qquad y = Ax + Bx^3; y = Y', N';\ x = v' \tag{26}$$

Compared with the model test results of the static drift test, the results of the CFD calculation in all the ranges show that the CFD results compare well with the experimental data. In Table 8, the relative errors for the calculated forces and moment are compared with experimental values at each drift angle. Table 9 shows the relative errors by comparing the hydrodynamic derivatives obtained from EFD calculated with the value of CFD in this study.

4.2 Pure sway simulation

It is possible to measure the force and the moment according to the change of sway velocity and the acceleration by generating sway force while the pure swaying test is performed. Only the variables of the acceleration-related were measured since the range of the sway velocity is narrower than static drift simulation. The results of pure sway simulation are shown in Figure 14, 15 and Table 9.

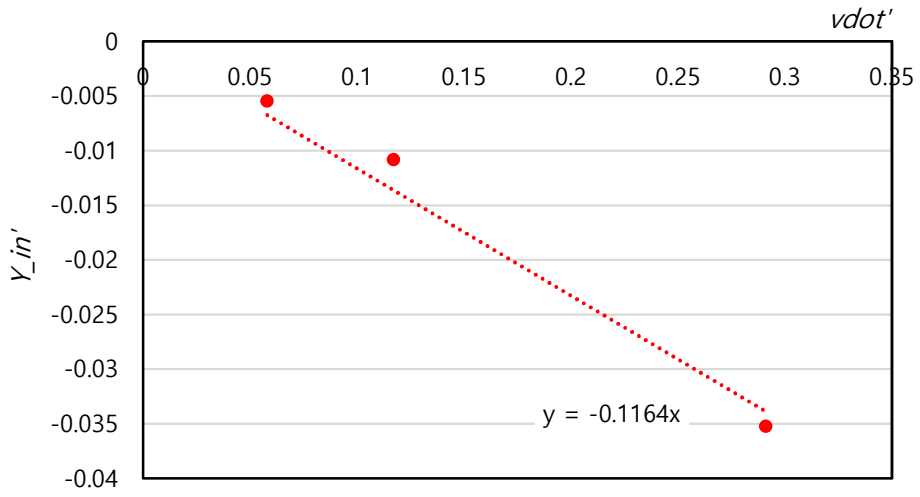

Figure 14. Non-dimensional in-phase sway force in pure sway

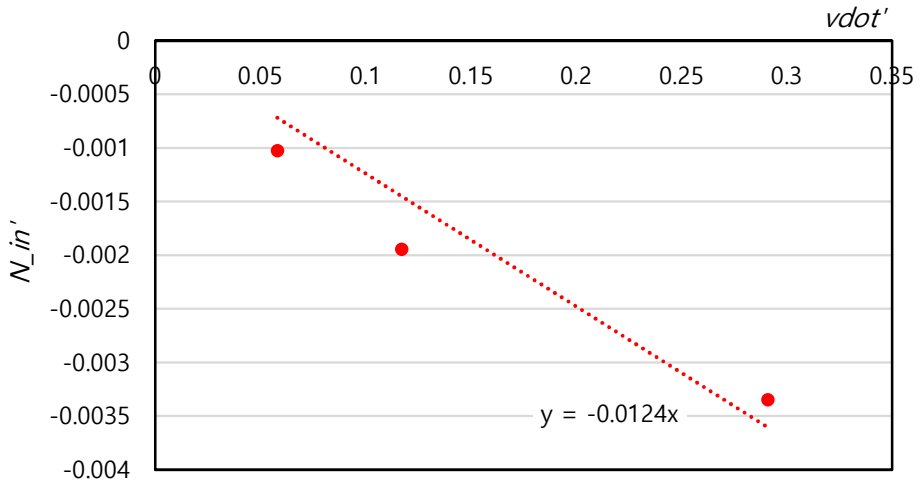

Figure 15. Non-dimensional in-phase yaw moment in pure sway

Table 9. Hydrodynamic derivatives in pure sway simulation and comparison with the EFD data

Derivatives	Present CFD	EFD (Yoon et al., 2009)	Error
$Y_{\dot{v}}'$	-0.1164	-0.1111	-1.48 %
$N_{\dot{v}}'$	-0.0124	-0.0131	7.39 %

For post processing, the zeroth and first order Fourier transformation and integration were applied. As a result of Pure sway simulations, the hydrodynamic derivatives calculated by CFD showed approximately 5% errors compared with the experiments. The hydrodynamic derivatives in Pure Sway Simulation were calculated using Equation 27.

$$y = Ax; y = Y', N'; \ x = \dot{v}' \qquad (27)$$

4.3 Pure yaw simulation

The Pure yaw simulations were conducted to derive the hydrodynamic derivatives of variable associated with the angular velocity (r). The model ship is always tangential on the trajectory of harmonic motion. The results of the comparison between the experimental data and present CFD results of force and moment and the hydrodynamic derivatives in the Pure Yaw simulations are shown in Figures 16, 17, 18 and Table 10.

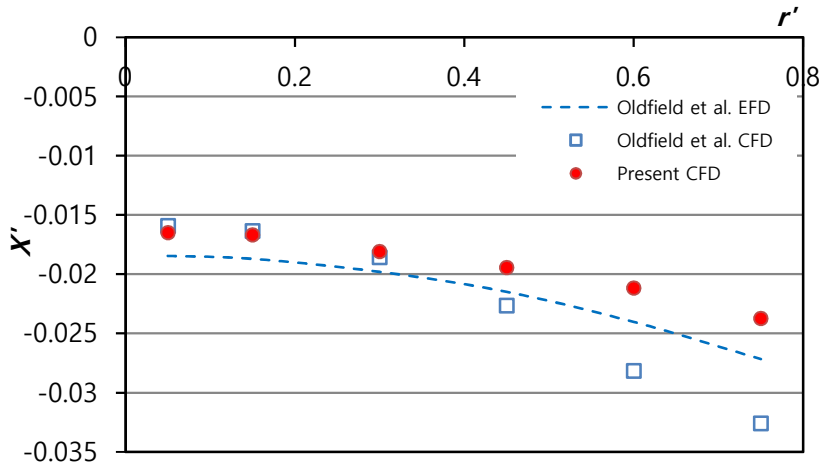

Figure 16. Non-dimensional surge force comparison in pure yaw

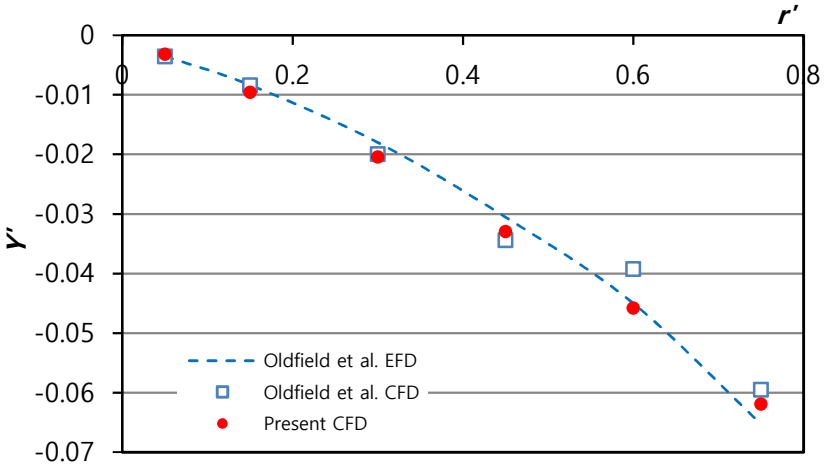

Figure 17. Non-dimensional sway force comparison in pure yaw

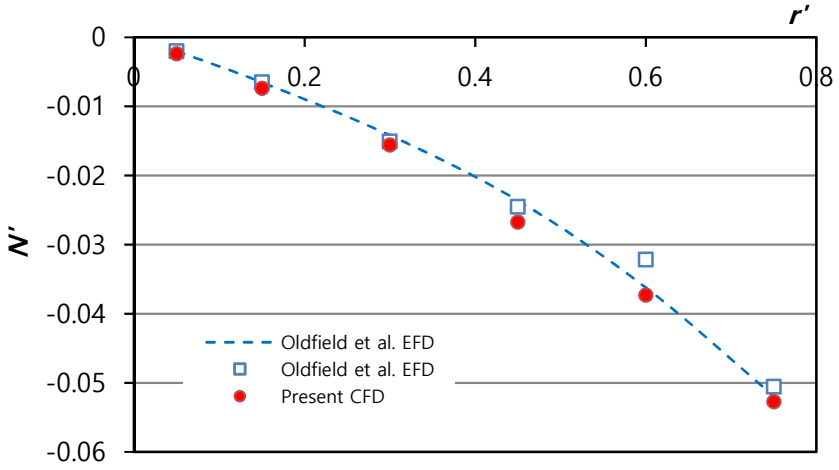

Figure 18. Non-dimensional yaw moment comparison in pure yaw

Table 10. Hydrodynamic derivatives in pure yaw simulation and comparison with the EFD data

Derivatives	Present CFD	EFD (Yoon et al., 2009)	Error
X_{rr}'	-0.01451	-0.0191	24.03 %
Y_r'	-0.06518	-0.0457	-42.63 %
Y_{rrr}'	-0.03239	-0.057	43.18 %
N_r'	-0.05033	-0.0487	-3.35 %
N_{rrr}'	-0.03533	-0.0342	-3.30 %
$Y_{\dot{r}}'$	-0.0198	-0.0136	-45.59 %
$N_{\dot{r}}'$	-0.01605	-0.0092	-45.59 %

For post processing, the zeroth and first order Fourier transformation and integration were applied. As a result of Pure yaw simulations, the simulated hydrodynamic derivatives by CFD have maximum 40% errors compared to the test results in terms of sway force. The hydrodynamic derivatives in Pure Yaw Simulation were calculated using Equation (28).

$$\begin{gathered} y = A + Bx^2; y = X';\ x = r' \\ y = Ax + Bx^3; y = Y', N';\ x = r' \\ y = Ax; y = Y', N';\ \dot{r}' \end{gathered} \tag{28}$$

4.4 Yaw with drift simulation

Yaw with Drift simulation was performed to obtain the coupled hydrodynamic derivatives of *v* and *r*. Simulations were performed with non-dimensional angular velocity of 0.3 and angles of 9, 10, and 11 degrees. The simulation results are shown in Figures 19, 20 and 21 it is shown in comparison with the model test results under the same conditions. Table 11 shows the results of the hydrodynamic derivatives calculations.

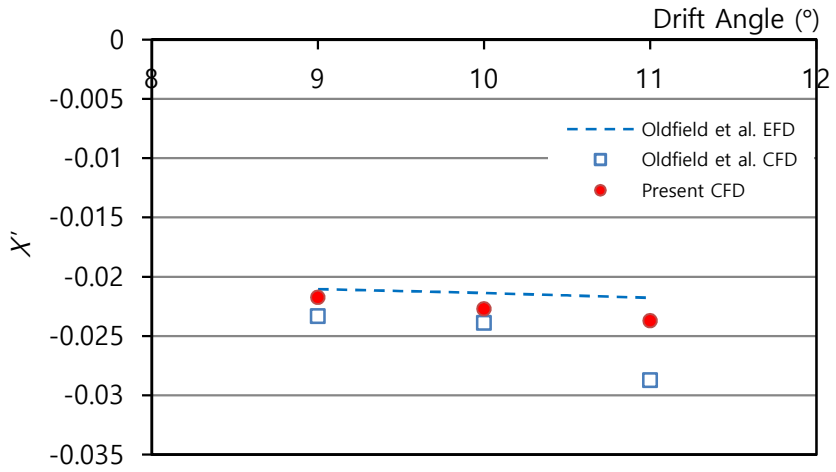

Figure 19. Non-dimensional surge force comparison in yaw with drift

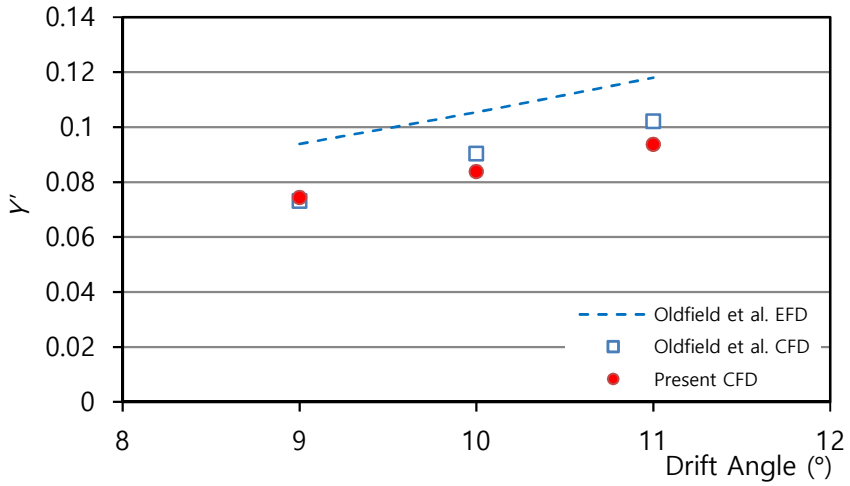

Figure 20. Non-dimensional sway force comparison in yaw with drift

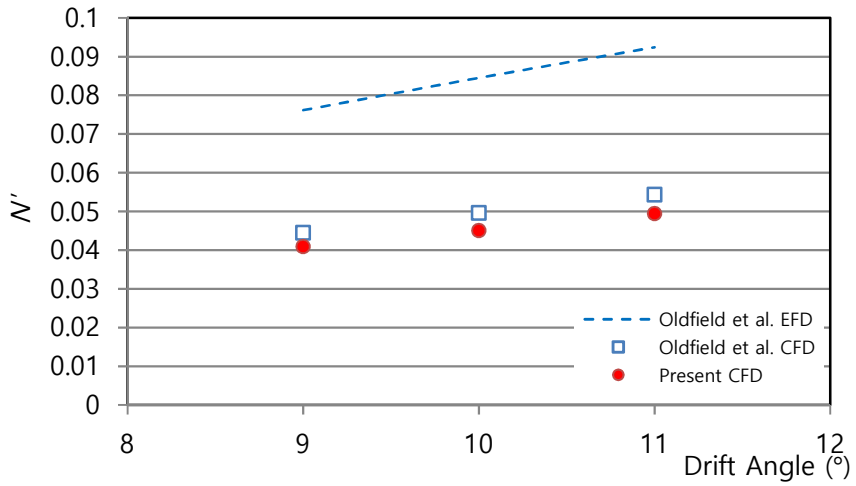

Figure 21. Non-dimensional yaw moment comparison in yaw with drift

Table 11. Hydrodynamic derivatives in yaw with drift and comparison with the EFD data

Derivatives	Present CFD	EFD (Yoon et al., 2009)	Error
X_{vr}'	0.0255	0.0300	14.98 %
Y_{vrr}'	-0.7913	-1.3683	42.17 %
Y_{rvv}'	-0.6680	-1.7067	60.86 %
N_{vrr}'	-0.3289	-0.4011	18.00 %
N_{rvv}'	-0.6353	-0.5512	-15.26 %

4.5 Simulation modelling

4.5.1 Introduction

Many simulation methods such as KIJIMA MMG MODEL, AOKI MMG MODEL based on MMG (Maneuvering Modelling Group) model to predict maneuverability of ship have been presented. Some of the simulation methods may be difficult to apply for obtaining hydrodynamic forces or moment in the maneuvering simulations since one method is not always applicable to other method in general. To overcome this issue, basic form of the method should exist. From this background, research committee on ‘‘standardization of mathematical model for ship maneuvering predictions’’ was organized by the Japan Society of Naval Architects and Ocean Engineers and proposed a standard MMG form for maneuvering prediction method. It is called ‘‘MMG standard method’’. In this article, turning and zigzag simulations are modelled using MMG standard method.

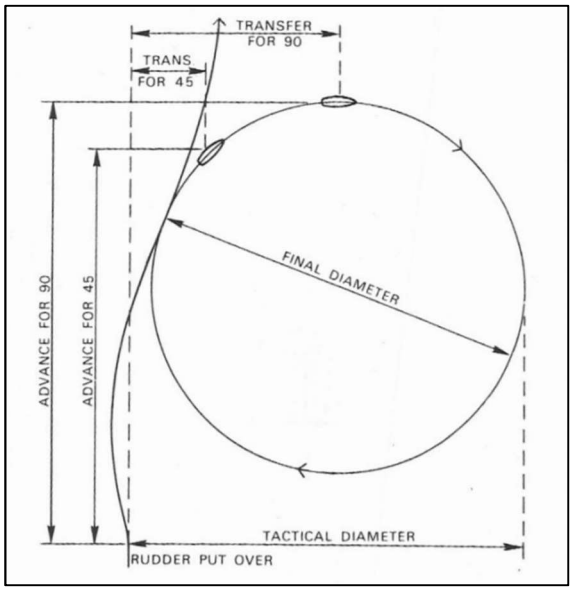

Figure 22. Definition of turning test

First, turning test is performed for predicting the turning ability. It is a method that has been used for a long time since it can check the turning ability of the ship intuitively. Figure 24shows the turning test. Generally, it runs straight at a constant speed and then turns the rudder angle to $35°$. Propeller RPM is controlled constantly until the turning angle of the ship turns $360°$. The heading angle, the speed of the ship and the trajectory of the ship are recorded during the turn test. The advance distance and the tactical diameter are used as a measure of turning ability. The advance distance is the distance in the x direction which advances until the heading angle of the vessel is $90°$ after the rudder is operated. The tactical diameter is the distance until the heading angle of the vessel becomes $180°$. The advance distance is the minimum distance required to avoid obstacles in front of the ship by

turning, and the tactical diameter is derived from that $180°$ rotation of the ship for minimal movement is crucial for naval tactics. This is an important indicator of the turning ability of the ship. IMO regulates (Daidola et al, 2002) that the advance distance should be less than 4.5 times the length of the ship and that the tactical diameter should be less than 5 times the length of the ship.

Zigzag test is a test to evaluate the course changing ability of a ship. After the rudder turns $10°$, when the heading turns at $10°$, the rudder turns to $-10°$. When the heading angle of the ship is $-10°$, the rudder angle goes back to $10°$. It is called zigzag test making zigzag movement by turning. Even if it turns the rudder in the opposite direction to the turning ship, the ship does not turn in the opposite direction immediately. In this case, the angle after turning rudder in opposite direction is called the overshoot angle. The first overshoot angle and the second overshoot angle are used as a measure to determine the course changing ability. The larger the overshoot angle, the worse the course changing ability. If the course keeping ability get worse the overshoot angles become larger.

4.5.2 Simulation model algorithm

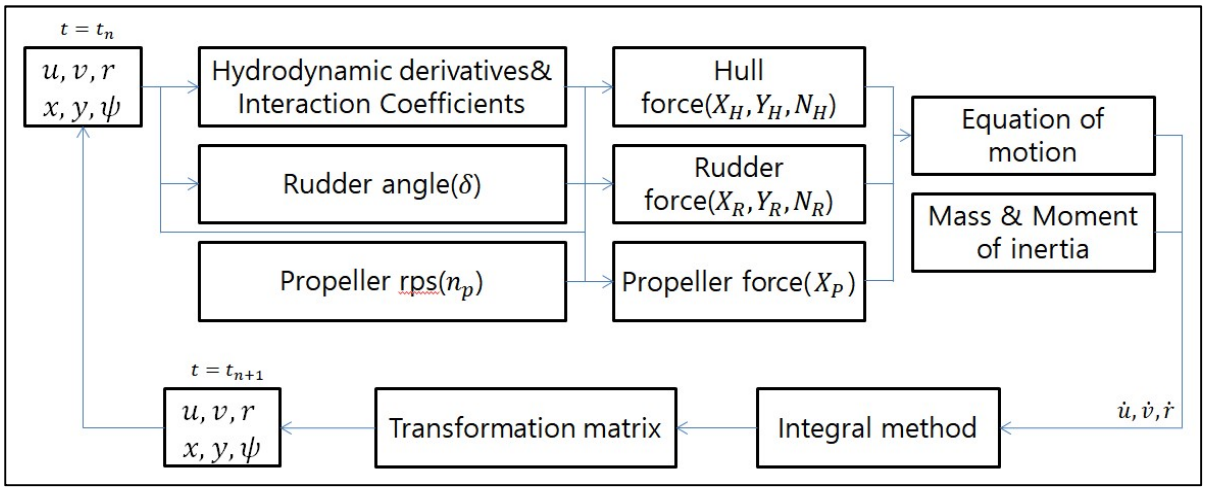

Figure 23. Algorithm of maneuvering simulator

In this study, simulation models were constructed using Simulink, a simulation environment development program, to analyse the maneuvering performance through numerical simulation. The algorithm of the simulation model is depicted in Figure 22.

As shown in Figure 22, the force acting on hull, rudder, and propeller are calculated using the velocity, angular velocity of the ship at each time interval (t_n). The Equation of motion is calculated by using the calculated external force and the inertial term of the ship. Through this, the acceleration, angular acceleration and turning angle of the ship are derived for each direction. It is possible to calculate the velocity and angular velocity, heading angle of the ship at t_{n+1} using previous velocity and angular velocity, heading angle. The position of the vessel in the earth fixed coordinate system is also calculated by converting the corresponding velocity, angular velocity and heading angle.

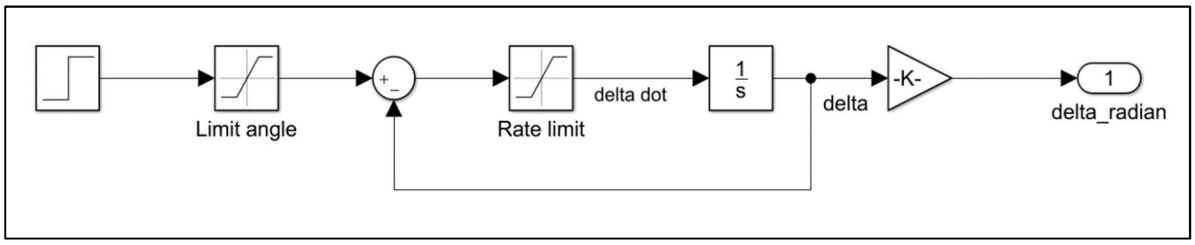

Figure 24. Simplified diagram of rudder command

The modelling of rudder angle (δ) commend in the simulation is shown in Figure 23. This is a simple block diagram of the principle of steering.

$\dot{\delta}$ represents the rudder angular velocity. The maximum rudder angle is limited by the limit angle box and the maximum angular velocity is limited by the rate limit box to efficiently simulate the actual steering. The velocity of the ship (U) based on the ship fixed coordinate system with the origin at the midship is modelled as expressed in Equation (29).

$$U = \sqrt{u^2 + v_m^2} \tag{29}$$

In order to model the motion Equations which are mentioned in this paper in a convenient form, the acceleration for each direction is modelled as shown in Equation (30) and applied to the simulation.

$$\dot{u} = \frac{X'}{(m' + m'_x)}\left(\frac{U^2}{L}\right)$$

$$\dot{v} = \frac{(I'_{zG} + x'^2_G m' + J'_z)Y' - (m' x'_G)N'}{det(M)}\left(\frac{U^2}{L}\right) \tag{30}$$

$$\dot{r} = \frac{-(x'_G m')Y' + (m' + m'_y)N'}{\det(M)}\left(\frac{U^2}{L^2}\right)$$

$$\det(M) = (m' + m'_y)(I'_z + x'^2_G m' + J'_z) - (x'^2_G m'^2)$$

The ship's position x, y and ψ for the Earth's fixed coordinate system are obtained from the transformation matrix expressed by Equation (31). The model is constructed so that the position of the ship can be derived by integrating the acceleration value.

$$\dot{x_0} = (u' cos\psi - v'_m sin\psi)U$$

$$\dot{y_0} = (u' sin\psi + v'_m cos\psi)U \tag{31}$$

$$\dot{\psi} = r' \frac{U}{L}$$

In this study, the angular acceleration and angular acceleration are integrated for every time step.

4.5.3 Result of simulation model

In order to verify the constructed simulation model, the validation simulation was performed using the data of Dash et al. (2015). Maneuvering simulations were conducted for turning test and zigzag test to predict ship's turning ability and course changing ability.

In this study, the advance distance and the tactical diameter are used for predicting the turning ability, and the 1st and 2nd overshoot angles are used for checking the course changing ability. After making Simulink structure, the hydrodynamic derivatives were inserted from paper of Dash et al. (2015). Figures 25, 26, 27 and Table 12 show the simulation result.

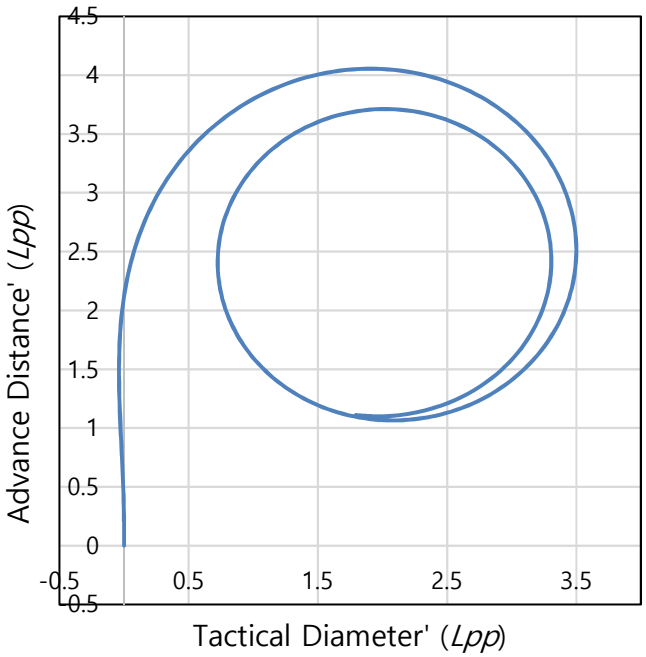

Figure 25. 35 Degree turning simulation

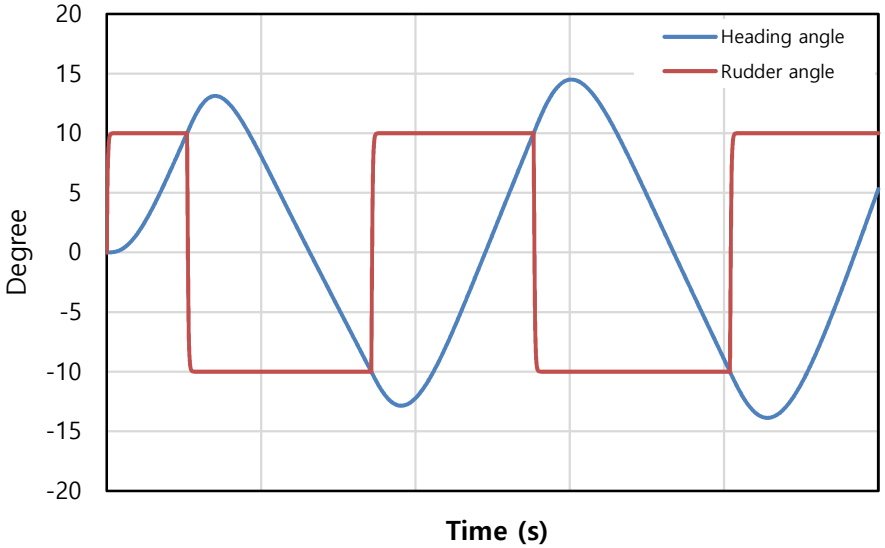

Figure 26. 10/10 Zigzag simulation

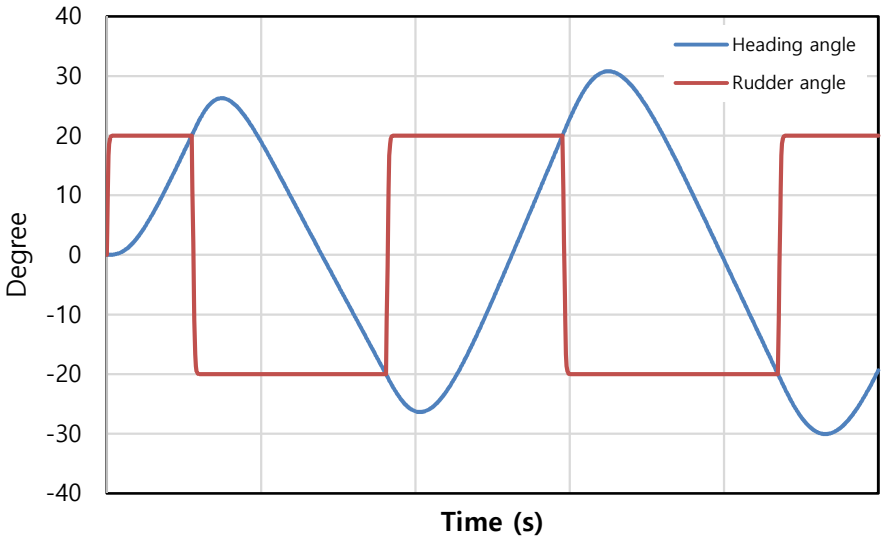

Figure 27. 20/20 Zigzag simulation

After performing simulations, 20/20 Zigzag simulation results were compared with Dash et al.'s paper to validate Simulink structure. 35 degree turning simulation and 10/10 zigzag were not compared since there is no data publicly available.

Table 12. Comparison in 20/20 zigzag simulation

20/20 Zigzag	Dash et al. (2015)	Present Structure
1st Overshoot	5.29 °	6.27 °
2nd Overshoot	5.11 °	4.20 °

Finally, the hydrodynamic derivatives from CFD in this study were inserted on the Simulink structure and the results are presented in Table 13.

Table 13. Result of turning & zigzag simulation

35 Turning	Simulation Result	10/10 Zigzag	Simulation Result	20/20 Zigzag	Simulation Result
Advance Distance	2.53 L_{PP}	**1st Overshoot**	1.08 °	**1st Overshoot**	2.53 °
Tactical Diameter	4.73 L_{PP}	**2nd Overshoot**	0.95 °	**2nd Overshoot**	3. 00 °

5 Conclusion and future work

CFD simulations have been performed numerically using Planar Motion Mechanism (PMM) model tests of the DTMB 5415 with bilge keels. The aim of this study is to validate the accuracy of CFD simulation and practicality of MMG model to predict the ship maneuvering with CFD result.

The CFD simulations include 9 cases of static drift, 3 cases of pure sway, 6 cases of pure yaw, and 3 cases of yaw with drift corresponding SIMMAN 2012 model test specification. Grid convergence studies including three grid sizes were completed at 20° static drift in terms of force and moment. Details such as the vessel geometry, physical condition, model scale, and Equations were extracted from SIMMAN 2012 proceeding. The analysis was focused on the non-dimensional hydrodynamic derivatives for predicting ship maneuvering.

When it comes to static drift simulation, the relative errors compared with the experimental data are between 0.3 and 5.0 percent. And the linear hydrodynamic derivatives exhibit 0.8~8.0 percent error. Even though the error is low enough, nonlinear hydrodynamic derivatives such as Y_{vvv}, N_{vvv} have relatively high errors up to 26%. In fact, it shows that nonlinear value has high sensitivity more than linear value. In pure sway simulation, two derivatives, $Y_{\dot{v}}, N_{\dot{r}}$, are obtained. Another derivative related lateral velocity also can be obtained. However, these types of derivatives were calculated in static drift simulation since static drift simulation has wider lateral velocity range. The error of derivatives is 1.0~7.0 percent. In terms of pure yaw simulation, it has similar tendency to static drift simulation that linear derivatives were well matched whereas nonlinear derivatives higher error. Especially, there was a higher error about sway force. Lastly, in yaw with drift simulation, it also shows higher error up to twice in terms of sway force. The simulation has higher drift angle, the noise of sway force is getting bigger. It is shown that the nonlinearity influences on the CFD result. The natural phenomenon has high portion for calculation result. To have more accurate results, the grid size should be made smaller and the time-step should be reduced. It is considered that the error due to nonlinearity influence the MMG simulation. The results of Simulink simulation illustrated difference compared with existing paper.

For the future work, appendage ship model need to be used for virtual captive model test. Because, the hydrodynamic forces and moments acting on rudder and propeller are important part in terms of predicting maneuverability. Considering appendage is one of the ways to implement real phenomenon as possible. Another way is simulating using full scale model. In the present paper, all simulations conducted with model scale ship. Even though Froude number is matched, Reynolds number is hard to match with full scale's one. Thus, full scale simulation is expected more accurate result. Uncertainty analysis also needs for checking the accuracy of simulation condition.

Reference

Daidola, J. C., Lundy, W. & Barr, R., 2002. "Evolution of the Standards for Maneuverability.", SNAME Transactions, Volume Vol. 110, pp. pp. 395-411.

Dash, A. K., Nagarajan, V. & Sha, O. P., 2015. ''Uncertainty assessment for ship maneuvering mathematical model.", International Shipbuilding Progress, Volume 62, p. 57–111.

Duman, S., Sezen, S., Bal, S., 2017. "URANS Approach in Hull-Propeller-Rudder Interaction of a Surface Combatant at High Speed.", Napoli, 11st SYMPOSIUM ON HIGH SPEED MARINE VEHICLES.

Hajivand, A. & Mousavizadegan, H. S., 2015. "Virtual maneuvering test in CFD media in presence of free surface.", International Journal of Naval Architecture and Ocean Engineering, 7(3), pp. 540-558.

ITTC, M. C. o. t. 2., 2017. "ITTC – Recommended Procedures and Guidelines, Guideline on Use of RANS Tools for Manoeuvring Prediction.", Wuxi: 28th ITTC 2017.

K., A. & F, S., 2008. "SIMMAN 2008 workshop on verification and validation of ship maneuvering simulation methods.", Copenhagen, SIMMAN 2008 Workshop Proceedings.

Kim, Y. G., Kim, S. Y., Kim, H. T., Lee, S. W., 2006. "Studying on Maneuvering Characteristic of a Container Ship with Twin Skeg.", Journal of the Society of Naval Architects of Korea, 43(1), pp. 15-21.

Benedetti et al., 2007. "PMM MODEL TEST WITH DDG51 INCLUDING UNCERTAINTY ASSESSMENT.", Rome: INSEAN.

Lee, S.-K., Lee, G.-W. & Lee, S.-J., 1997. "A Study on the Prediction of Maneuvering Motion for a Twin-Screw Twin-Rudder ship at Initial Design Stage.", Journal of Korean Navigation and Port Research, 21(1), pp. 103-108.

MAN Diesel & Turbo, 2007. https://marine.mandieselturbo.com/docs/librariesprovider6/technical-papers/propulsion-trends-in-lng-carriers.pdf?sfvrsn=18. [Online].

Oldfield, C. & Larmaei, R., 2015. "Prediction of Warship Manoeuvring Coefficients using CFD", Ottawa: STX Marine., External Literature.

Otzen, J. F. & Simnonsen, C. D., 2014. "SIMMAN 2014 workshop on verification and validation of ship maneuvering simulation methods.", Copenhagen, SIMMAN 2014 Workshop Proceeding.

Phillips, A., Furlong, S. & Turnock, R., 2007. "Virtual planar motion mechanism tests of the autonomous underwater vehicle autosub.", At STG-Conference / Lectureday "CFD in Ship Design" STG-Conference / Lectureday "CFD in Ship Design". 26 Sep 2007. 8 pp.

Simonsen, C. D., Otzen, J. F., Klimt, C. & Larsen, N. L., 2012. "Maneuvering predictions in the early design phase using CFD generated PMM data.", Gothenburg, 29th Symposium on Naval Hydrodynamics, pp. 26-31.

Tezdogan, T. et al., 2015. "Full-scale unsteady RANS CFD simulations of ship behaviour and performance in head seas due to slow steaming.", Ocean Engineering, Volume 97, pp. 186-206.

Will, G., John, B., Jeremy, A. & Andrew, J., 2013. "An Investigation into Twin Skeg Hullforms In Auxiliary Tanker Design.", Barton, ACT: Engineers Australia.

Yasukawa, H. & Yoshimura, Y., 2015. "Introduction of MMG standard method for ship maneuvering predictions.", Journal of Marine Science and Technology, 20(1), pp. 37-52.

Yoon, H., 2009. "Phase-Average Stereo-PIV Flow Field and Force/Moment/Motion Measurements for Surface Combatant in PMM Maneuvers.", Iowa, The University of Iowa.

Zou, L., Larsson, L. & Orych, M., "2010. Verification and validation of CFD predictions for a manoeuvring tanker.", Journal of Hydrodynamics, Ser. B 22(5), pp. 438-445.

Appendix

A. Static drift test

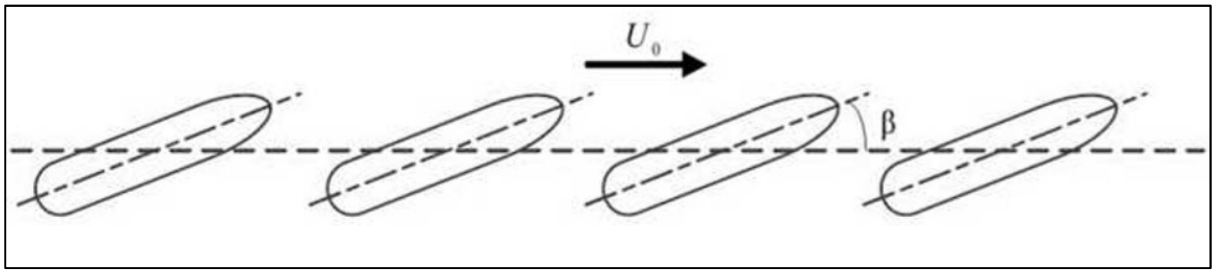

Figure 28. Methodology of satic drift test

When the model ship is towed by changing the drift angle β as shown in Figure 28, the force and moment acting on the hull at each drift angle can be measured. The drift angle is expressed as Equation (32) of function of the lateral velocity.

$$v = -U_0 sin\beta$$
$$v' = -sin\beta \quad (32)$$

The force and moment measured for each condition are expressed as a function of the polynomial Equation as shown in Eq. (33). $X_{vv}, Y_v, Y_{vvv}, N_v\ N_{vvv}$ are predicted using this Equation.

$$X'_{mean} = X'_0 + X'_{vv} \cdot v'^2$$
$$Y'_{mean} = Y'_0 + Y'_v \cdot v' + Y_{vvv} \cdot v'^3 \quad (33)$$
$$N'_{mean} = N'_0 + N_v' \cdot v'\_N_{vvv} \cdot v'^3$$

Here, the subscript mean means the value obtained by averaging the force and moment over time of the measured data.

B. Pure sway test

In the PMM test, the harmonic motion test is a test in which the model ship is towed and the harmonic motion is performed, and the hydrodynamic force acting at this time is measured to obtain the hydrodynamic derivatives The PMM test is a general model test used in many research institutes because it has the advantage of simultaneously measuring additional mass force, additional moment of inertia and damping force. The zero and first order Fourier integration methods of the measured data signal are used to separate the dynamical added mass force and the additional moment of inertia from the damping force in pure sway test and pure yaw test. There is another method, but this study only refers to the Fourier integral method using in this study.

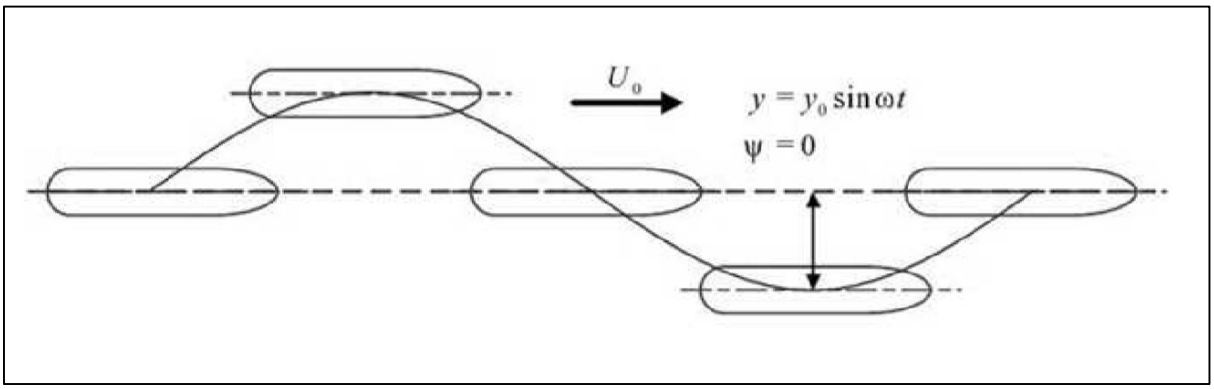

Figure 29. Methodology of pure sway test

The pure sway test is shown in Figure 29. If the initial phase of the pure sway is assumed to be zero, then the motion as the following Equation (34) occurs.

$$X = U_0 t$$
$$Y = y_0 \, sin(wt) \tag{34}$$
$$\psi = 0$$

$\rightarrow$ u = U_0, $v_m = y_0 \omega cos(wt)$, $r = 0$, $\dot{u} = 0$, $\dot{v} = -y_0 \omega^2 sin(wt)$, $\dot{r} = 0$

$\rightarrow$ $u' = 1/\sqrt{1 + k^2 \, cos^2(wt)}$, $v' = kcos(wt)/\sqrt{1 + k^2 \, cos^2(wt)}$, $r' = 0$

$\dot{u}' = 0$, $\dot{v}' = -(L/y_0)k^2 sin(wt)/1 + k^2 \, cos^2(wt)$, $\dot{r}' = 0$

$k = \frac{y_0 \omega}{U_0}$

Since the sway displacement is $y = y_0 sinwt$,, the signal of the sway force measured according to this motion can be expressed as $Y_{measured} = Y_0 + Ysin(wt - \epsilon)$. In this case, Y_0 means the mean value of the measured signal, and ϵ is the phase difference between the sway displacement and the measured signal. Thus, the in-phase and out-phase are separated into $Y_{measured}, N_{measured}$ Can be expressed as Equation (35), (36).

$$\begin{aligned} Y_{measured} &= Y_0 + Ysin(wt - \epsilon) \\ &= Y_0 + Ycos\epsilon\ sinwt - Ysin\epsilon\ coswt \\ &= Y_0 + Y_{In} sinwt - Y_{out} coswt \end{aligned} \tag{35}$$

$$\begin{aligned} N_{measured} &= N_0 + Nsin(wt - \epsilon) \\ &= N_0 + Ncos\epsilon\ sinwt - Nsin\epsilon\ coswt \\ &= N_0 + N_{In} sinwt - N_{out} coswt \end{aligned} \tag{36}$$

Where Y_{In} and N_{In} are the additional mass and inertia moments and inertia forces with the same phase as the displacements, and Y_{out}, N_{out} are the damping forces with the $90°$ phase difference. The measured signal, which can be expressed separately as in the above Equation, is Fourier transformed for T in one period, and the integrated form is shown in following Equation. Fourier transformation and integration are performed in the same way for pure sway force and pure yaw force, so only the process for sway force is described as Equation (37).

$$\begin{aligned} \int_0^T Y_{measured} dt &= \int_0^T Y_0 dt + \int_0^T Y_{In} sinwtdt + \int_0^T Y_{out} coswtdt = TY_0 \\ \int_0^T Y_{measured} sinwtdt &= \int_0^T Y_0 sinwtdt + \int_0^T Y_{In} \sin^2 wtdt + \int_0^T Y_{Out} coswtsinwt\, dt \\ &= \int_0^T Y_{In} \sin^2 wtdt = \frac{T}{2} Y_{In} \\ \int_0^T Y_{measured} coswtdt &= \int_0^T Y_0 coswtdt + \int_0^T Y_{In} sinwt\ coswtdt + \int_0^T Y_{Out} \cos^2 wtdt \\ &= \int_0^T Y_{Out} \cos^2 wtdt = \frac{T}{2} Y_{Out} \end{aligned} \tag{37}$$

In the pure swaying test, it is possible to derive the additional mass force and the additional moment of inertia and the inertial force on the same phase by Fourier sine transformation and integration for one period when the function of the y direction displacement is sine function.

On the other hand, damping force can be derived by Fourier cosine transformation and integration. In this study, the damping force term can be measured for a larger range through the static drift test. Therefore, only the hydrodynamic derivatives related to the additional mass force and the additional moment of inertia is obtained.

C. Pure yaw and yaw with drift test

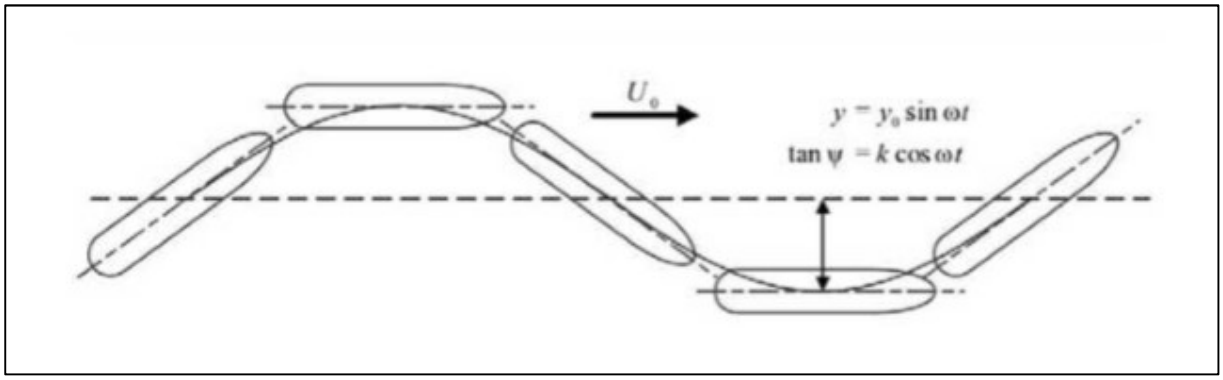

Figure 30. Methodology of pure yaw test

Figure 30 outlines the motion obtained through a pure yaw test. The pure yaw test is a motion in which the heading angle is tangent to the forced movement of model ship. If a drift angle is applied to the pure yaw test, the test is a yaw and drift test. The hydrodynamic derivative which is combined with lateral velocity and angular velocity can be obtained by the test. The pure sway test and the yaw with drift test are performed by the following Equation (38), and when $\beta = 0$, the test is a pure yaw test.

$$\begin{aligned} X &= U_0 t \\ Y &= y_0 sin(wt) \\ tan(\psi - \beta) &= k cos(wt) \end{aligned} \tag{38}$$

$\rightarrow u = U_0 cos\beta \sqrt{1 + k^2 cos^2(wt)}$,

$v_m = -U_0 sin\beta \sqrt{1 + k^2 cos^2(wt)}$

$r = -kwsin(wt)/\{1 + k^2 cos^2(wt)$

$$\dot{u} = -\frac{U_0 k^2 w sin(wt)\, cos(wt)}{\sqrt{1+k^2\, cos^2(wt)}} cos\beta$$

$$\dot{v} = \frac{U_0 k^2 w sin(wt)\, cos(wt)}{\sqrt{1+k^2\, cos^2(wt)}} sin\beta$$

$$\dot{r} = -\frac{\{kw^2\, cos(wt)\}\{1+k^2+k^2\, sin^2(wt)\}}{\{1+k^2\, cos^2(wt)\}^2}$$

$$u' = cos\beta,\ v'_m = -sin\beta,\ r' = -\left(\frac{kwL}{U_0}\right)\frac{sin(wt)}{\{1+k^2\, cos^2(wt)\}^{1.5}},\ k = \frac{y_0 w}{U_0}$$

In the case of the pure yaw test, the additional mass force and the additional moment of inertia force can be derived from the same phase hydrodynamic force, and the damping force can be derived from the opposite phase hydrodynamic force. The description of Fourier transforms and integration is the same as the above-mentioned method. Therefore, it will not be described again. Table 14 summarizes the data signals measured by the PMM test in terms of the force and moment for the in-phase and the out-phase.

Table 14. Analysis of PMM test corresponded hydrodynamic derivatives

PMM Test	Pure sway	Pure yaw
Motion(Input)	$y = y_0\, sin(wt)$ $v = y_0 w cos(wt)$ $\dot{v} = -y_0 w^2 sin(wt)$	$\psi = \psi_0 sin(wt)$ $r = \psi_0 w cos(wt)$ $\dot{r} = -\psi_0 w^2 sin(wt)$
Motion eq. (Output)	$Y_{m\cdot} = Y_0 - (m + m_y)\dot{v} + Y_v v_m + Y_{vvv} v_m^3$ $N_{m\cdot} = N_0 + N_v v_m + N_{vvv} v_m^3$	$Y_{m\cdot} = Y_0 + (Y_r - m)r + Y_{rrr} r^3$ $N_{m\cdot} = N_0 - (I_z + J_z)\dot{r} + N_r r + N_{rrr} r^3$
Hydrodynamic derivatives	$Y_{In} = -(m + m_y)\dot{v}$	$N_{In} = -(I_z + J_z)\dot{r}$ $Y_{Out} = (Y_r - m)r + Y_{rrr} r^3$ $N_{Out} = (N_r - m x_G)r + N_{rrr} r^3$